Multi-source Least-squares Reverse Time Migration with Topography

Dongliang Zhang[*1], *Ge Zhan*[2] *and Gerard T. Schuster*[1], *1. King Abdullah University of Science and Technology, 2. BP*

SUMMARY

We demonstrate an accurate method for calculating LSM images from data recorded on irregular topography. Our results with both the Marmousi and Foothill models with steep topography suggest the effectiveness of this method.

INTRODUCTION

Multisource least squares reverse time migration (MLSRTM) has been proven to be cost-effective in improving the spatial resolution of migration images for marine data (Dai et al., 2010, 2011, 2012). One of the key requirements is a sufficiently accurate migration velocity model. Implicit in LSRTM is also the need for a sufficiently accurate forward modeling algorithm, even in the presence of a rough topographic surface (Graves, 1996; Robertsson, 1996; Levander, 1988; Hestholm and Ruud, 1998; Zhang and Chen, 2006; Zhang et al., 2012) for a land survey or an OBS experiment with a variable sea floor elevation. Modeling seismic waves with rough topography can induce artificial diffractions at the free surface, which will introduce erroneous reflectors in the migration image. To avoid such problems, we develop a finite-difference algorithm that accurately models acoustic waves with topographic slopes. It is based on the ghost extrapolation method previously used for modeling electromagnetic waves in a conductive medium (Zhang, 2011) and modeling fluid flow fields in fluid mechanics (Frederic and Ronald, 2005). We now show that this modeling procedure can be successfully used with MLSRTM for acoustic models with a variable topography Results with synthetic data for a steeply dipping free surface show no noticeable artifacts in the modeling or migration images.

This paper is organized into four sections. The first part is this introduction, followed by the theory section for least squares migration and the ghost extrapolation method. The third section presents results for migrating synthetic data generated from models with a roughly varying topography. The final part presents conclusions.

THEORY

Least-squares Reverse Time Migration

Least squares reverse time migration (LSRTM) iteratively finds the reflectivity model that iteratively minimizes the waveform misfit function by gradient optimization method. The LSRTM algorithm and its implementation are described as follows.

1.The misfit function is defined as:

$$f(\mathbf{m}) = \frac{1}{2}||\mathbf{Lm}-\mathbf{d}||^2, \tag{1}$$

where, $\mathbf{m}$ is the reflectivity model, $\mathbf{L}$ is the Born modeling operator that predicts multiples and $\mathbf{d}$ is the recorded data.

2. The misfit gradient $\mathbf{g}$ is defined as:

$$\mathbf{g} = \mathbf{L}^T[\mathbf{L}(\mathbf{m})-\mathbf{d}], \tag{2}$$

where, $\mathbf{L}^T$ is the adjoint of $\mathbf{L}$. This equation denotes the reverse time migration of the residuals.

3. Once the gradient is known, the reflectivity distribution can be iteratively updated by the, for example, steepest descent method:

$$\mathbf{m}^{k+1} = \mathbf{m}^k - \alpha\mathbf{g}^k, \tag{3a}$$

$$\alpha = \frac{(\mathbf{g}^k)^T\cdot\mathbf{g}^k}{(\mathbf{Lg}^k)^T\cdot\mathbf{Lg}^k}, \tag{3b}$$

where, k is the iteration number and α is the step length. At each iteration, the residual multiples are migrated by reverse time migration to compute the gradient and the reflectivity is updated by the steepest descent method with the step length α. The iterative procedure is stopped when the data residual falls below a specified limit.

Multi-source Phase-encoding

The misfit gradient calculation in equation 2 for least-squares migration is similar to RTM, where the misfit gradient is

$$g(x,z) = \sum_{\omega} S^*(x,z,\omega)R(x,z,\omega), \tag{4}$$

where $S(x,z,\omega)$ and $R(x,z,\omega)$ represent the source and residual wavefields, $g(x,z)$ is the misfit gradient at (x,z), * represents the complex conjugate, and the summation represents the zero-lag correlation. There is a significant computational speedup if the summation is carried out over all (or partial) shot gathers before applying this imaging condition (Romero et al., 2000; Krebs et al., 2009; Zhan et al., 2010; Dai et al., 2011). That is, instead of single shot gathers for $R(x,z,\omega)$ and $S(x,z,\omega)$, we replace them by a sum of phase encoded shot gathers so that the composite (or multi-source) wavefields are defined as

$$\tilde{S}(x,z,\omega) = \sum_{j=1}^{N} a_j(\omega)S_j(x,z,\omega), \tag{5}$$

and

$$\tilde{R}(x,z,\omega) = \sum_{j=1}^{N} a_j(\omega)R_j(x,z,\omega), \tag{6}$$

where N is the number of shot gathers combined together, and a_j is the phase-encoding factor. However, this approach introduces crosstalk when we insert equations 5 and 6 into equation

SEG Houston 2013 Annual Meeting
DOI http://dx.doi.org/10.1190/segam2013-0270.1

4:

$$\begin{aligned}\tilde{g}(x,z) &= \sum_{\omega}\tilde{S}^{*}(x,z,\omega)\tilde{R}(x,z,\omega)\\ &= \sum_{j=1}^{N}\sum_{\omega}|a_j(\omega)|^2 S_j^{*}(x,z,\omega)R_j(x,z,\omega)+\\ &\sum_{j\neq k}^{N}\sum_{k=1}^{N}\sum_{\omega}\overbrace{a_j^{*}(\omega)a_k(\omega)S_j^{*}(x,z,t)R_j(x,z,t)}^{crosstalk}. \quad (7)\end{aligned}$$

If the phase-encoding factors are orthogonal (i.e.,$a_j a_k = \delta_{jk}$), then the first summation in equation 7 reduces to the correct misfit gradient (equation 4). However, the phase-encoding terms are typically not orthogonal so the unwanted $j \neq k$ cross-terms (the second term in equation 7) are unphysical cross-correlations between unrelated source and residual wavefields. If these crosstalk terms are strong enough then they produce an unacceptable migration result.

Finite-Difference Modeling with Ghost Extrapolation

In the multi-source LSM method, it is important to accurately model wavefields for sources near a free-surface with an irregular topography. To implement the boundary condition on irregular topography, we propose the ghost extrapolation method. The acoustic wave equation

$$\frac{\partial^2 P}{\partial x^2}+\frac{\partial^2 P}{\partial z^2}=\frac{1}{v^2}\frac{\partial^2 P}{\partial t^2}, \quad (8)$$

for a model with a free-surface boundary condition means that the pressure is zero on the surface, where P is the pressure and v is the velocity. The fourth-order finite-difference scheme requires the center point to have two points along each of the four directions shown in Figure 1. When the center point is close to the surface, some of these points extend above the free surface, and we call these points the ghost points (see Figure 1). Considering the z direction (see Figure 2a), so the differencing scheme can be written as

$$\begin{aligned}\frac{\partial^2 P}{\partial z^2} = &-\frac{1}{12}P_{i-2,j}+\frac{4}{3}P_{i-1,j}-\frac{5}{2}P_{i,j}+\\ &+\frac{4}{3}P_{i+1,j}-\frac{1}{12}P^{G}_{i+2,j}, \quad (9)\end{aligned}$$

where i, j are the nodal indices and the superscript G indicates this point is the ghost point above the free surface. The key issue is how to compute the value of the ghost points in order to calculate the second-order derivative of the pressure at this point. Physically, the pressure of the ghost point in the air should be zero. In this case, the virtual value of the ghost point can be estimated by using a polynomial extrapolation method. That is, assume that the wavefield near the surface is a local cubic function

$$\tilde{P}(z) = az^3+bz^2+cz+d, \quad (10)$$

where a, b, c and d are the coefficients, and then select the four points to calculate these coefficients. It is extremely important that the selected four points contain a point on the free boundary to satisfy the boundary condition. The second step is to extrapolate the pressure to the ghost point utilizing a cubic interpolation polynomial. With the ghost point values, the second-order derivative in the z direction of the points near the surface can be calculated. This procedure is repeated for the ghost points in the x (Figure 2b) and z directions. This extrapolation method can be improved by using polynomials that are functions of all three coordinate variables x, y, and z, but we will restrict our tests to one-dimensional interpolation.

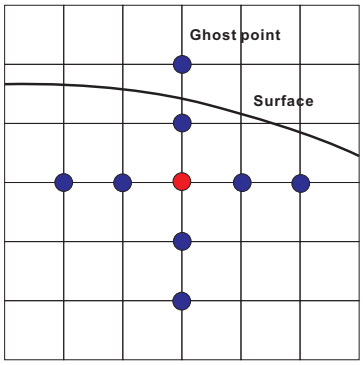

Figure 1: The fourth-order scheme, where the center point is near the surface and the FD stencil extend above the free surface; these extended points are called ghost points.

The ghost extrapolation does not require an approximation to the surface topography, so it will not generate diffractions for those when the standard finite-difference method is used. As an example, Figure 3 shows a simple dipping surface model and Figure 4a shows the common shot gather computed by a finite-difference (FD) scheme with the ghost point extrapolation method. In comparison, Figure 4b depicts the common shot gather computed by a FD method with the commonly used image boundary condition, and obvious diffractions can be seen. Finally, Figure 4c shows the common shot gather computed by a FD method with a vacuum free-surface condition, and obvious diffractions also can be seen.

NUMERICAL EXAMPLES

In this section, we test multi-source LSRTM with rough topography imposed on the Marmousi and the Foothill models. The observed data are generated by a FD Born modeling method.

Marmousi Model

The traditional Marmousi model has been modified by adding an irregular surface with peaks and valleys. The model size is 201×400 gridpoints with a grid spacing of 5 m. There are 200 shots and 400 receivers with the 25 Hz Ricker wavelet. Figure 5a shows the true velocity model, Figure 5b shows the smooth velocity model for migration and Figure 6a presents the reflectivity model. 200 shot gathers are encoded and summed into one super gather, which significantly reduces the cost of calculation. However, there is strong crosstalk noise as shown in Figure 6b after 10 iterations. To suppress crosstalk, 80 iterations are used to get the final LSRTM image without crosstalk noise in Figure 6c.

Foothill Model

DOI http://dx.doi.org/10.1190/segam2013-0270.1

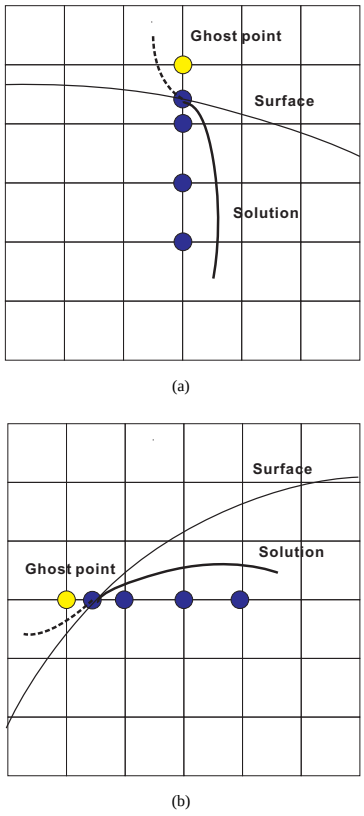

Figure 2: Diagram for gridpoint of the ghost extrapolation method. a) Ghost extrapolation in the z direction. We assume the solution near the surface is a local cubic function, then choose four blue points to calculate the coefficients of the cubic function; then extrapolate the pressure to the yellow point. b) The ghost extrapolation in the x direction is the same as that for the z direction.

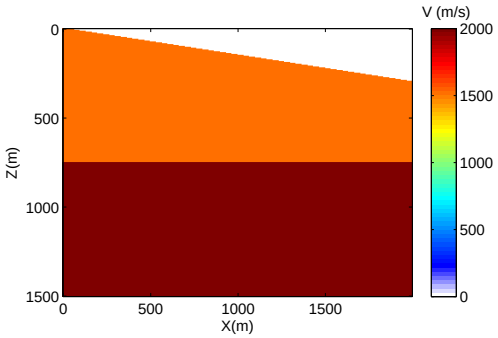

Figure 3: Two layer dipping surface model.

We test multi-source LSRTM with topography on the Foothill model that includes significant topography and velocity variations. The model size is 333×833 gridpoints with a grid spacing of 10 m. There are 208 shots and 833 receivers with the 15-Hz Ricker wavelet. Figure 7a shows the true velocity model, Figure 7b depicts the smooth velocity model for migration, and Figure 8a shows the reflectivity model. 208 shot

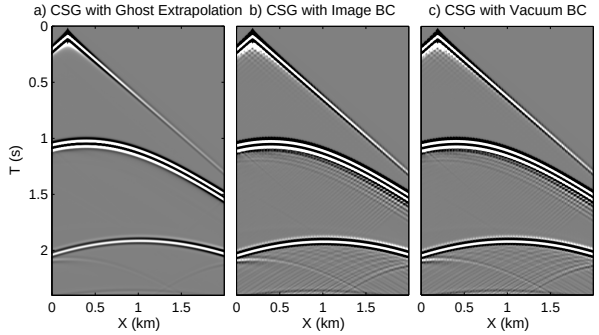

Figure 4: Common shot gathers computed by different FD modeling methods. a) Using the ghost extrapolation method, where there are no diffractions. The CSGs computed by FD methods that use b). image boundary conditions and c). vacuum boundary conditions (BC) show obvious diffractions.

gathers are encoded into one super gather, which can reduce the cost of calculation. However, there is significant crosstalk noise in the LSRTM image after 10 iterations (see Figure 8b). To suppress this crosstalk noise, we use 80 iterations to get the final LSRTM image without crosstalk in Figure 8c.

CONCLUSIONS

We demonstrate a method for calculating LSM images from data recorded on irregular topography. Our results with both the Marmousi and Foothill models with steep topography suggest its effectiveness in avoiding artificial reflections generated by forward modeling of wavefields on free surfaces with rough topography.

ACKNOWLEDGEMENTS

We thank the KAUST Supercomputing Lab for the computer cycles they donated to this project. We are especially grateful for the use of the SHAHEEN supercomputer. We also acknowledge the support of the CSIM sponsors (http://csim.kaust.edu.sa).

DOI http://dx.doi.org/10.1190/segam2013-0270.1

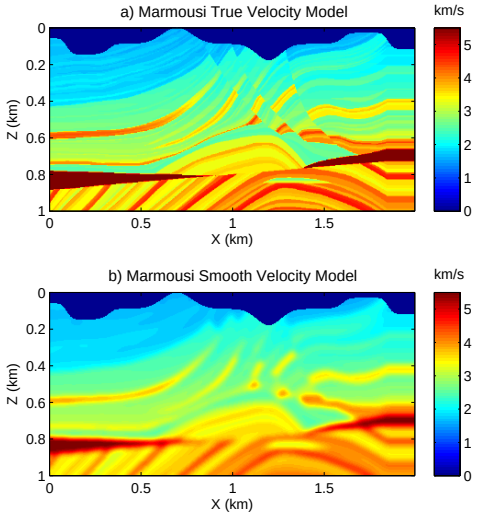

Figure 5: a) The true and b) smooth Marmousi velocity models with topography.

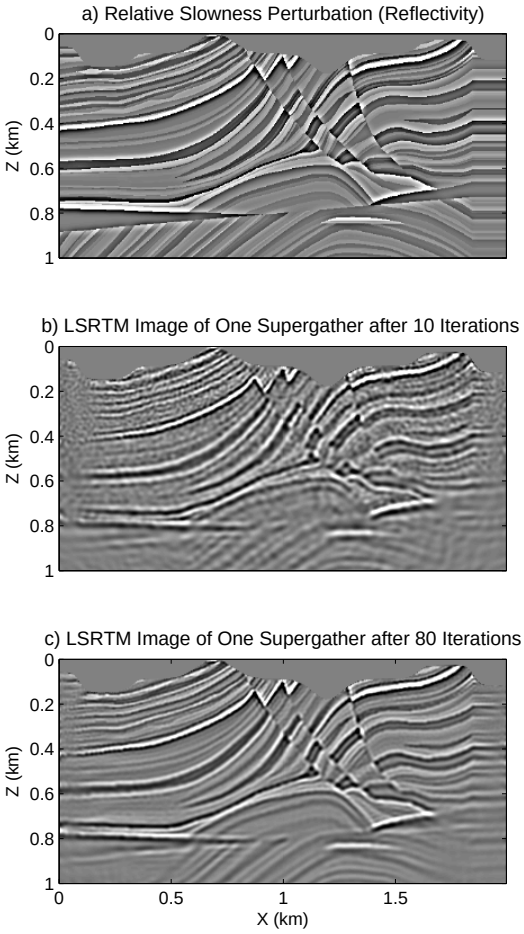

Figure 6: a) The Marmousi reflectivity model. The LSRTM images obtained from one super gather after b) 10 iterations and c) 80 iterations.

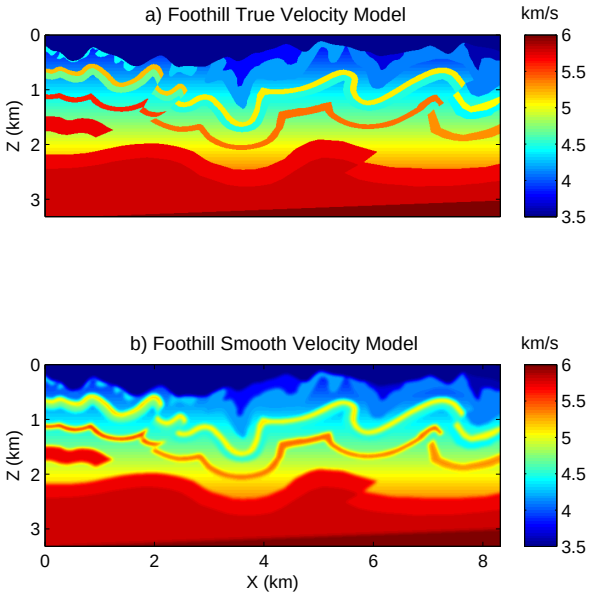

Figure 7: a) The true and b) smooth Foothill velocity model with topography.

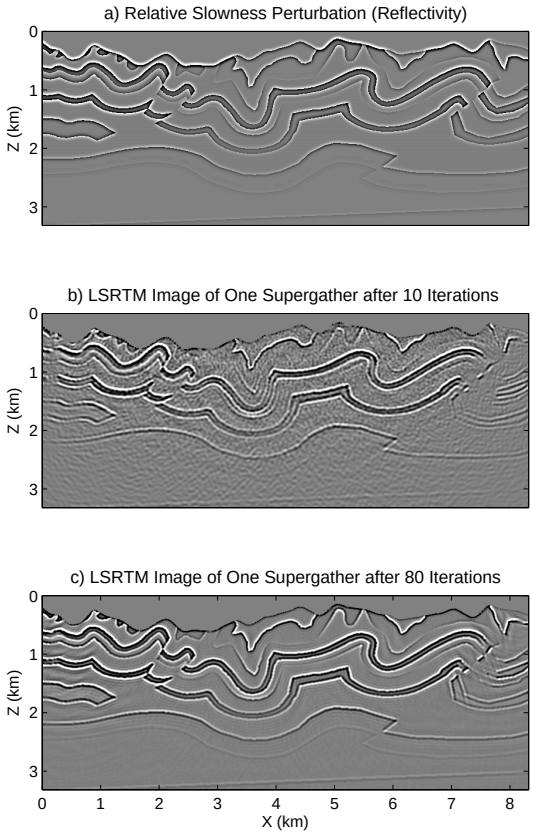

Figure 8: a) The Foothill reflectivity model. The LSRTM images of one super gather after b) 10 iterations and c) 80 iterations.

DOI http://dx.doi.org/10.1190/segam2013-0270.1

http://dx.doi.org/10.1190/segam2013-0270.1

EDITED REFERENCES

Note: This reference list is a copy-edited version of the reference list submitted by the author. Reference lists for the 2013 SEG Technical Program Expanded Abstracts have been copy edited so that references provided with the online metadata for each paper will achieve a high degree of linking to cited sources that appear on the Web.

REFERENCES

Dai, W., C. Boonyasiriwat, and G. T. Schuster, 2010, 3D multisource least-squares reverse time migration: 80th Annual International Meeting, SEG, Expanded Abstracts, **611**, 3120–3124.

Dai, W., P. Fowler, and G. T. Schuster, 2012, Multisource least-squares reverse time migration: Geophysical Prospecting, **60**, no. 4, 681–695, http://dx.doi.org/10.1111/j.1365-2478.2012.01092.x.

Dai, W., X. Wang, and G. T. Schuster, 2011, Least-squares migration of multisource data with a deblurring filter: Geophysics, **76**, no. 5, R135–R146, http://dx.doi.org/10.1190/geo2010-0159.1.

Frederic, G., and F. Ronald, 2005, A fourth order accurate discretization for the laplace and heat equations on arbitrary domains, with applications to the Stefan problem: Journal of Computational Physics, **22**, 577–601.

Graves, R., 1996, Simulating seismic wave propagation in 3D elastic media using staggered-grid finite difference: Bulletin of the Seismological Society of America, **86**, 1091–1106.

Hestholm, S., and B. Ruud, 1998, 3D finite-difference elastic wave modeling including surface topography: Geophysics, **63**, 613–622, http://dx.doi.org/10.1190/1.1444360.

Krebs, J. R., J. E. Anderson, D. Hinkley, R. Neelamani, S. Lee, A. Baumstein, and M.-D. Lacasse, 2009, Fast full-wavefield seismic inversion using encoded sources: Geophysics, **74**, no. 6, WCC177–WCC188, http://dx.doi.org/10.1190/1.3230502.

Levander, A. R., 1988, Fourth-order finite-difference p-sv seismograms: Geophysics, **53**, 1425–1436, http://dx.doi.org/10.1190/1.1442422.

Robertsson, J. O. A., 1996, A numerical free-surface condition for elastic/viscoelastic finite-difference modeling in the presence of topography: Geophysics, **61**, 1921–1934, http://dx.doi.org/10.1190/1.1444107.

Romero, L. A., D. C. Ghiglia, C. C. Ober, and S. A. Morton, 2000, Phase encoding of shot records in prestack migration: Geophysics, **65**, 426–436, http://dx.doi.org/10.1190/1.1444737.

Zhan, G., W. Dai, C. Boonyasiriwat, and G. T. Schuster, 2010, Acoustic multi-source waveform inversion with deblurring: 72nd Annual International Conference and Exhibition, EAGE, Extended Abstracts, G002.

Zhang, D., 2011, Finite difference modeling of dc electrical field including undulate topography: Ph.D. thesis, Jilin University.

Zhang, D., G. Zhan, and W. Dai, 2012, Multisource full waveform inversion with topography using ghost extrapolation: International Geophysical Conference and Oil & Gas Exhibition, 162, 1–4.

Zhang, W., and X. Chen, 2006, Traction image method for irregular free surface boundaries in finite difference seismic wave simulation: Geophysical Journal International, **167**, no. 1, 337–353, http://dx.doi.org/10.1111/j.1365-246X.2006.03113.x.